

Incompleteness of graph convolutional neural networks for points clouds in three dimensions

Sergey N. Pozdnyakov^{1,*} and Michele Ceriotti^{1,†}

¹*Laboratory of Computational Science and Modelling, Institute of Materials, Ecole Polytechnique Fédérale de Lausanne, Lausanne 1015, Switzerland*

(Dated: January 19, 2022)

Graph convolutional neural networks (GCNN) are very popular methods in machine learning, and have been applied very successfully to the prediction of the properties of molecules and materials: atoms form the vertices of a graph, and bonds are the edges connecting them. This first-order approach is known to be *incomplete*, i.e. there are graphs that are distinct, but appear identical when seen through the lens of the GCNN. More complicated schemes have thus been designed to increase the resolving power. Applications to molecules (and more generally, point clouds), however, add a geometric dimension to the problem. Edges can be decorated with the distance between atoms, and the resulting “distance graph convolution NNs” have empirically demonstrated excellent resolving power, and are widely used in chemical ML. Here we show that, even for the restricted case of graphs induced by 3D atom clouds, dGCNNs are not complete. We construct pairs of distinct point clouds that are, for any cutoff radius, indistinguishable by first-order graph convolutions that rely on node labels and distance-labelled edges. This class of degenerate structures include chemically-plausible configurations, setting an ultimate limit to the expressive power of some of the well-established GCNN architectures for atomistic machine learning. Models that explicitly use angular information in the description of atomic environments can resolve these degeneracies.

I. INTRODUCTION

Point clouds can be used to provide an abstract description of shapes, and objects across different length scales,^{1,2} and have been widely used in the construction of machine-learning models for computer vision³, remote sensing⁴ and autonomous driving⁵. A description in terms of an unordered set of points is relevant also at the atomic scale, where molecules and materials are most naturally characterised in terms of the position and nature of their atomic constituents. The list of Cartesian coordinates of points, however, does not reflect the fact that the properties associated with a given structure are usually invariant, or equivariant, to symmetry operations such as rigid translations, rotations, or permutation of the ordering of the points. In the context of atomistic simulations, the problem of describing a structure in a symmetry-adapted manner has been a central concern in early applications of machine-learning models^{6–8}, and has since given rise to the development of a large number of *representations* that attempt to characterize fully a structure while simultaneously fulfilling the requirements of symmetry⁹.

In fact, deep connections are present between most of the existing frameworks¹², that differ in implementation details but can be understood as describing structures in terms of unordered lists of distances, angles, tetrahedra, etc. within atom-centered environments, corresponding to correlations between 2, 3, 4, ν neighbors of the central atom. This systematic study has revealed that – at least for low values of ν – atom-centered representations are *incomplete*, i.e. there are pairs of structures that are distinct, but which contain environments that are indistinguishable based on the unordered list of distances and angles¹¹, which also affects the ability of the representa-

tion to resolve local deformations of certain structures¹³. This issue is also closely related to classical problems in invariant theory¹⁴, that aim to determine under which conditions two point clouds can be unequivocally identified by the unordered list of distances, or distances and angles. The impact of these degeneracies on machine-learning models of atomic and materials properties is mitigated by the fact that structures that contain problematic environments usually also contain others that are not degenerate, and so a model that *simultaneously* uses information on all centers can still distinguish the structures.¹⁵ For instance, all structures in Fig. 1 except for (b) can be discriminated by knowledge of the set of unordered list of distances around each point (i.e. taking $\{|\mathbf{r}_i - \mathbf{r}_j|\}_{j \in A}\}_{i \in A}$. Still, there is evidence that the incompleteness of atom-density representations does affect the ultimate performance of the machine-learning models built on them.¹¹ This is therefore an issue of practical, and not only theoretical, relevance, which is driving a transition towards systematically-improvable features with higher correlation order^{12,16–18}.

In the broader context of models based on point clouds, graph convolutional neural networks (GCNN) have been used extensively to describe the relative arrangement of points, mapping the cloud onto a graph.^{3,19} In the case of atomistic models, most well-established CNN frameworks treat atoms as the vertices of the graph, labeled by their chemical identity, and the edges are associated with the distances between them.^{20–22} Even though this class of “distance graph convolution” NN (dGCNN) only uses information on the distances between points, the way this is combined in the subsequent steps of the network allows for very flexible models with considerable descriptive power. It is well-known that for general discrete graphs it is possible to build pairs of items that are distinct,

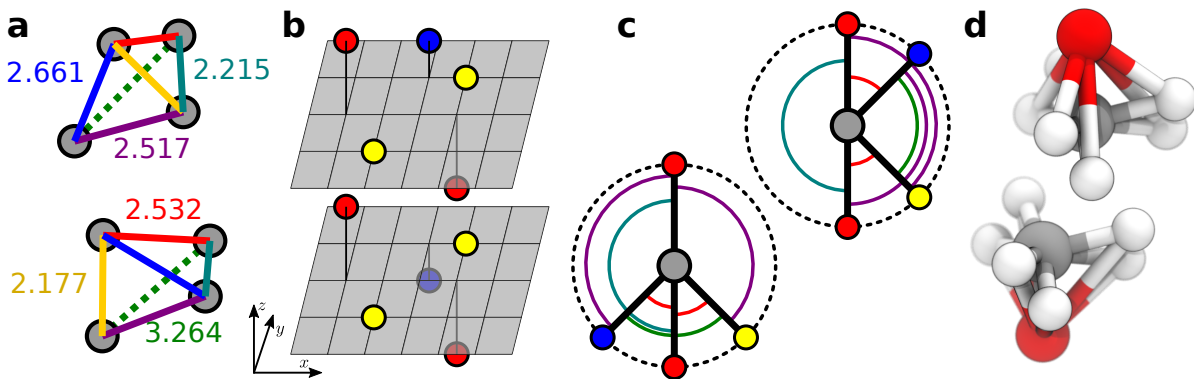


FIG. 1. Examples of structures (a,b), or environments (c,d) that are distinct but cannot be discriminated by the unordered list of distances or distances and angles between the points. (a) The two tetrahedra share the same list of pair distances, as per color coding.¹⁰ (b) The two structure share the same list of pair distances, and the list of distances of each atom relative to its neighbors. (c) The two environments share the same list of distances and angles relative to the central (gray) atom. (d) The two environments share the same list of distances, angles and dihedrals around the central (gray) atom.¹¹

and yet indistinguishable by most traditional GCNN.²³ This has triggered the development of higher-order graph networks²⁴. To the best of our knowledge, however, no examples have been shown of 3D point clouds whose fully-connected, distance-labelled graphs cannot be resolved by a dGCNN. In fact, dGCNNs can discriminate between the known examples of environments that are degenerate under $\nu = 1, 2, 3$ atom-centered descriptors, including all those shown in Fig. 1, suggesting a higher descriptive power. Here we present a class of point clouds involving pairs of structures that are not distinguishable by dGCNN. We show that this construction includes also configurations that correspond to realistic chemical structures, and demonstrate how for these configurations there is a limit to the accuracy that can be reached by this class of models.

II. WESFEILER-LEHMAN TEST FOR GEOMETRIC GCNNs

The Wesfeiler-Lehman test is a well-known graph-theoretical procedure^{25,26} that provides a sufficient condition for two graphs being distinct, and that has been shown to be equivalent to an assessment of the resolving power of several classes of GCNNs^{23,27,28}. Here we use a version of the test that incorporates explicitly the distances between nodes in the construction of the node identifiers, and is similar in spirit to the construction of graph kernels in Ref. 29. Given a set of n nodes with labels, $\{l_i\}_{i=1\dots n}$, and distances between them and their neighbors $\{r_{ij}\}$, we construct fingerprints of each node as the multiset of label/distance pairs, supplemented with a label of the node

$$h_i = \text{hash}(l_i, \{\{(l_j, r_{ij})\}_{j=1\dots n}\}). \quad (1)$$

The hash function assigns a unique identifier to distinct multisets. The values of the hashes are then used to

re-label the nodes, and the procedure is iterated: the process of encoding in the node labels the structure of the neighborhood and then iterating the procedure has a clear analogy with message passing constructs. Usually (but not always) the procedure converges; if the multiset of hashes that characterize two graphs is identical, the graphs cannot be distinguished by this distance-decorated W-L test, and won't be discriminated by a geometric dGCNN that uses only point labels and pair distances to characterize graph neighborhoods.

III. A COUNTEREXAMPLE

Consider the construction in Figure 2a. Six points, with labels that are identical in pairs, are arranged following the pattern in the figure, forming two structures, A^+ and A^- . The structures are periodic along the x axis, with a period p , and have open boundary conditions along y and z . After one iteration of the modified W-L procedure discussed in Section II, one sees that the unordered set of distances for V/V' , W/W' , C/C' pairs are identical, so that the plain and primed points will receive the same hash value, and the two graphs cannot be discriminated by the test despite being different (Figure 2b). The essential ingredient to induce a degeneracy is the swapping of the distances between C and W points, i.e. that $d(C^+, W) = d(C^-, W')$ and $d(C^+, W') = d(C^-, W)$, which is a consequence of the regular spacing of the points along the x axis and the periodic boundary conditions. It is important to stress that even though we only show minimum-image distances in the figure, the graphs generated by the periodic structure are degenerate even when considering a fully-connected graph, including all distances between periodic replicas.

Failure in distinguishing graphs based on the W-L test indicates that the pairs are equivalent to a broad

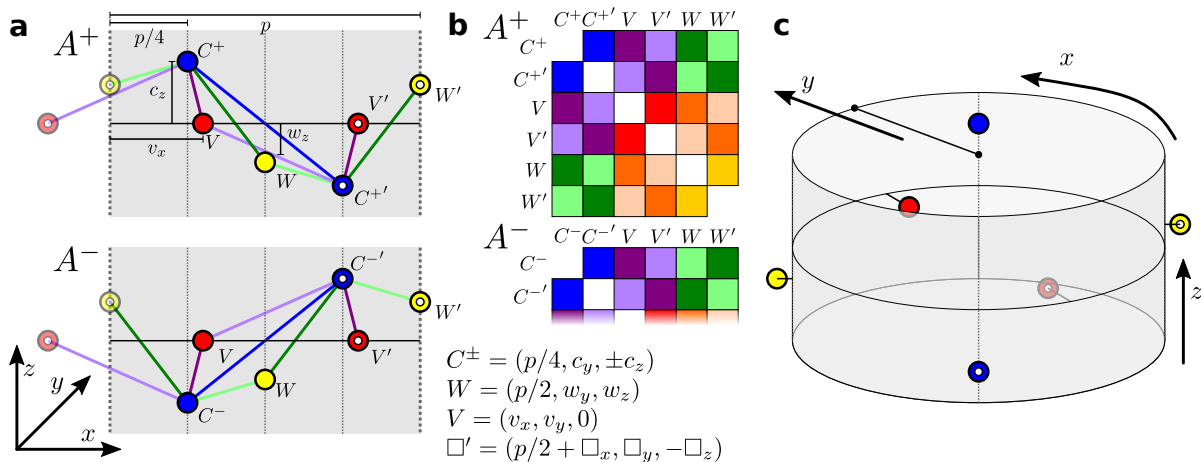


FIG. 2. (a) Two structures, A^+ , A^- that generate pair-distance graphs that are indistinguishable based on a W-L test. Both structures are periodic along x , and the coordinates of the six points are given in the figure: the points have the same label in pairs; V and W points are identical in the two structures, while C points are reflected relative to the xy plane. Distances involving the C^\pm points are highlighted, using a minimum image convention along the periodic direction. (b) Euclidean adjacency matrices between the points in the A^+ and A^- structures. The two matrices differ only by the order of the $C - W$ distances. V and V' have the same set of edge distances, and so the W/W' and C^\pm/C'^\pm pairs: thus, from the point of view of the W-L test, there are only three types of nodes and the graphs are indistinguishable. (c) A finite pair of degenerate structures can be obtained by wrapping the period around the z axis and embedding the periodic structure in Euclidean 3D space.

class of pair-distance GCNNs,²⁰ that includes SchNet²¹, convolutional-networks molecular fingerprints³⁰, molecular graphs convolutions³¹, graph networks³², and many others. As a special case, the A^\pm structures in Fig. 2a are also degenerate with respect to the *full set* of neighbor-distances multisets, which means they are an example for which $\nu = 1$ atom-centered features cannot discriminate *globally* between the two structures. In this sense, this is a much more difficult case than the degenerate tetrahedra in Fig. 1a, which have the same set of distances but can be easily distinguished when considering the triplets of distances associated with the vertices, and of the scheme in Fig. 1b, which is globally undistinguishable by $\nu = 1$ representations, but can be resolved by a dGCNN.

This construction can be generalized in several different ways. Arbitrarily many pairs of V and W atoms, possibly with different labels, can be added to the two structures without breaking the degeneracy. Perhaps more intriguingly, it is possible to “fold” an arbitrary number P of repeat units of the structure around the z axis, to obtain a pair of finite structures embedded in 3D Euclidean space (Figure 2). If the coordinates in the x -periodic structure are $\{(x_i, y_i, z_i)\}$, the position of the finite-size structure are

$$\begin{aligned} r_i &= Pp/2\pi + y_i \\ \theta_i &= 2\pi x_i/pP \\ z_i &= z_i \end{aligned} \quad (2)$$

in a cylindrical coordinate system. This coordinate transformation works because it maps equal distances in the periodic structures to equal Euclidean distances in the

finite configurations, and so it does not affect the nature of the graphs, and their signature when subject to the W-L test. More in general, there is no reason to believe this to be the *only* family of degenerate structures that could be realized, based on a similar idea of generating configurations in which some distance pairs are swapped. Along these lines, it might be possible to find special cases that are degenerate also for convolution schemes that incorporate information about angles – such as equivariant neural networks³³, or higher-order graph neural networks^{24,34} – that have sufficient descriptive power to discriminate between the structures we introduce here.

IV. SIGNIFICANCE FOR CHEMICAL ML

The construction in Fig. 2 might seem somewhat contrived, but it is not difficult to use it to generate point clouds that correspond to realistic targets for machine learning. Consider for example the case of predicting the stability of molecular structures. Fig. 3 demonstrates two pairs of degenerate configurations corresponding to a water tetramer. Structure A_1^+ , in particular, is a mildly distorted version of the ground state configuration of $4\text{H}_2\text{O}$,³⁶ that we label as A_0 . The energies of these structures (which we computed at the B3LYP³⁷ level, using PySCF³⁸) are not absurd: the cohesive energies relative to four isolated H_2O molecules are $E_1^+ = -0.92$ eV, $E_1^- = 2.43$ eV, $E_2^+ = 0.39$ eV, $E_2^- = 2.07$ eV. Thus, in the best-case scenario a distance-based CNN can only predict the energies of $A_{1,2}^\pm$ with an RMSE of ≈ 1.3 eV. For

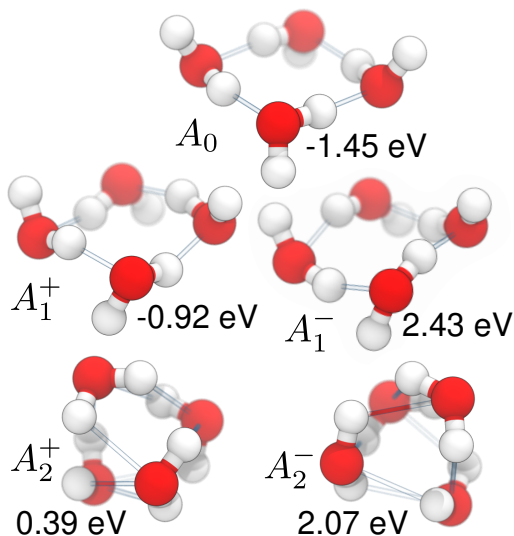


FIG. 3. A few configurations of a water tetramer that will be used as benchmarks. A_0 is the ground state structure for the tetramer³⁵. A_1^+ and A_2^+ are two structures that correspond to two periods of the 3D motif of Fig. 2c. The geometries of the $A_{1,2}^\pm$ structures have been obtained by a constrained minimization of the energy.

reference, the cohesive energy of the ground-state structure is $E_0 = -1.45$ eV, and the typical thermal energy at room temperature is 0.025 eV.

We train models of the cluster cohesive energy on a database of 10'000 water dimers and 5'000 water trimers (selected by farthest-point sampling, (FPS)³⁹ from the data set used in training the MB-pol potential^{40,41}) and 2'000 water tetramers configurations (FPS selected from a high-temperature Hamiltonian replica exchange simulation with a confining potential, performed using i-PT⁴² and the q-TIP4P/f forcefield⁴³). Energies were computed with the same B3LYP setup as for the degenerate structures. We show a comparison between a simple kernel model based on SOAP features¹⁰ (that incorporate two-neighbors correlations at the level of descriptors, and higher-order correlation through kernel non-linearity), and the SchNet framework²², a CNN that has been very successfully applied to several chemical ML problems⁴⁴⁻⁴⁸. We emphasize that we chose SchNet as a widespread CNN model, but *any* distance-based CNN that has a discriminating power equivalent to (or lower than) a first-order W-L test would exhibit the same problem. Similarly, we use a SOAP-based Gaussian Approximation Potential as a simple and well-understood scheme that incorporates explicitly angular information, but essentially any framework that does so would be capable of resolving the A^\pm degeneracy.

We use standard hyperparameters for both SchNet and the SOAP model. As shown in Fig. 4, the difference in behavior between the two schemes is qualitative. Both models can reduce monotonically the validation error on the n -mers dataset, but only the model that incorpo-

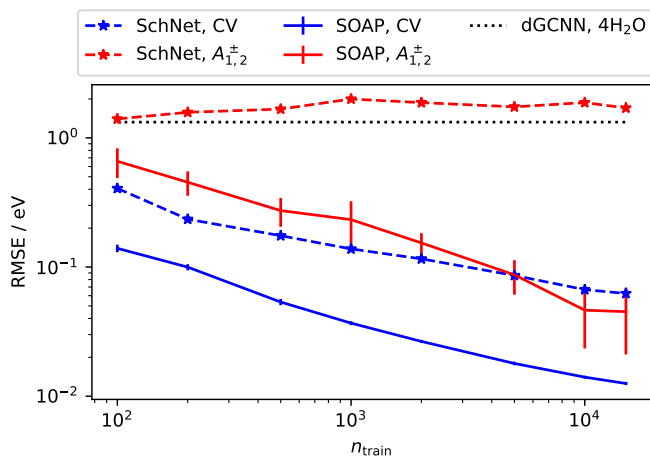


FIG. 4. Learning curves for SchNet (dashed lines) and SOAP GAP (full lines) models trained on a dataset of 2-, 3-, and 4-water clusters. Blue curves show validation error on a hold-out set of 2'000 structures, red curves the RMSE for the four $A_{1,2}^\pm$ geometries. The dotted black line corresponds to the ultimate limit for a dGCNN that cannot discriminate between the degenerate pairs.

rates angular information can tell the A^\pm pairs apart, and can bring the errors for $A_{1,2}^\pm$ below the theoretical limit for dGCNNs. The figure also shows that the two models exhibit very different CV performances, and that the SOAP-based kernel model yields a much larger error for $A_{1,2}^\pm$ than for the validation set, which does contain structures with a similar energy range. It is difficult to conclusively determine the reason for these observations, that depend at least in part on the details of the two models. One may hypothesize that structures that are only distinguishable by angular information may be more challenging for a SOAP model, and that even in the absence of structures that are *exactly* degenerate, the lack of resolving power of dGCNNs is reflected in a slower learning rate, similar to what was observed for two-neighbors degenerate structures in Ref. 11.

V. CONCLUSIONS

The idea of combining a characterization of point clouds in terms of graphs, where points are vertices and the connectivity is determined by point-to-point distances, with graph-convolution architectures has been extraordinarily successful in a broad range of applications of geometric machine-learning, and in particular in the construction of deep models of chemical structures, that lend themselves naturally to such description. Despite their simplicity, and despite the fact that general graphs that are indistinguishable based on this class of GCNN are known to exist, these frameworks have remarkable descriptive power for actual molecular geometries, being capable of discriminating between configurations that are degenerate to widely used atom-centered representations.

The construction we present here, that generates pairs of geometries that are indistinguishable when seen through the lens of a distance-GCNN, provides a counterexample that sets a limit to the accuracy that can be attained when regressing properties associated with the 3D point cloud. For the specific case of chemical machine learning, we show a concrete example that is of direct relevance to the chemistry of water clusters, demonstrating that the counterexample can have direct repercussions on practical applications.

Atom-centered descriptors that rely on correlations with at least two neighbors – as well as high-order graph convolution schemes and equivariant neural networks – are immune to this family of counterexamples. Determining rigorously the ingredients that must be incorporated in geometric machine learning to guarantee that an archi-

tecture can resolve arbitrary point clouds is a fascinating topic that touches upon several open problems in signal processing⁴⁹ and invariant theory.¹⁴ We hope that our data set will be used to test existing frameworks to determine empirically their descriptive power, and as the basis to extend our construction to break some of the higher order scheme schemes and to determine the simplest architecture that is not affected by this degeneracy.

ACKNOWLEDGMENTS

MC and SNP acknowledge support from the Swiss National Science Foundation [Project No. 200021-182057] and from the NCCR MARVEL, funded by the Swiss National Science Foundation (SNSF).

* These two authors contributed equally

† michele.ceriotti@epfl.ch

¹ S. Gumhold, X. Wang, R. S. MacLeod, *et al.*, in *IMR* (2001) pp. 293–305.

² Y. Guo, H. Wang, Q. Hu, H. Liu, L. Liu, and M. Benamoun, *IEEE Trans. Pattern Anal. Mach. Intell.* **43**, 4338 (2021).

³ W. Wu, Z. Qi, and L. Fuxin, in *2019 IEEE/CVF Conference on Computer Vision and Pattern Recognition (CVPR)* (IEEE, Long Beach, CA, USA, 2019) pp. 9613–9622.

⁴ S. A. Bello, S. Yu, C. Wang, J. M. Adam, and J. Li, *Remote Sensing* **12**, 1729 (2020).

⁵ Y. Li, L. Ma, Z. Zhong, F. Liu, M. A. Chapman, D. Cao, and J. Li, *IEEE Trans. Neural Netw. Learning Syst.* **32**, 3412 (2021).

⁶ J. Behler and M. Parrinello, *Phys. Rev. Lett.* **98**, 146401 (2007).

⁷ A. P. Bartók, M. C. Payne, R. Kondor, and G. Csányi, *Phys. Rev. Lett.* **104**, 136403 (2010).

⁸ M. Rupp, A. Tkatchenko, K.-R. Müller, and O. A. von Lilienfeld, *Phys. Rev. Lett.* **108**, 058301 (2012).

⁹ F. Musil, A. Grisafi, A. P. Bartók, C. Ortner, G. Csányi, and M. Ceriotti, *Chem. Rev.* **121**, 9759 (2021).

¹⁰ A. P. Bartók, R. Kondor, and G. Csányi, *Phys. Rev. B* **87**, 184115 (2013).

¹¹ S. N. Pozdnyakov, M. J. Willatt, A. P. Bartók, C. Ortner, G. Csányi, and M. Ceriotti, *Phys. Rev. Lett.* **125**, 166001 (2020).

¹² M. J. Willatt, F. Musil, and M. Ceriotti, *J. Chem. Phys.* **150**, 154110 (2019).

¹³ S. N. Pozdnyakov, L. Zhang, C. Ortner, G. Csányi, and M. Ceriotti, *Open Res Europe* **1**, 126 (2021).

¹⁴ M. Boutin and G. Kemper, *Advances in Applied Mathematics* **32**, 709 (2004).

¹⁵ O. A. von Lilienfeld, R. Ramakrishnan, M. Rupp, and A. Knoll, *Int. J. Quantum Chem.* **115**, 1084 (2015).

¹⁶ A. V. Shapeev, *Multiscale Model. Simul.* **14**, 1153 (2016).

¹⁷ R. Drautz, *Phys. Rev. B* **99**, 014104 (2019).

¹⁸ J. Nigam, S. Pozdnyakov, and M. Ceriotti, *J. Chem. Phys.* **153**, 121101 (2020).

¹⁹ Y. Wang, Y. Sun, Z. Liu, S. E. Sarma, M. M. Bronstein,

and J. M. Solomon, *ACM Trans. Graph.* **38**, 1 (2019).

²⁰ J. Gilmer, S. S. Schoenholz, P. F. Riley, O. Vinyals, and G. E. Dahl, in *International Conference on Machine Learning* (2017) pp. 1263–1272.

²¹ K. T. Schütt, H. E. Sauceda, P.-J. Kindermans, A. Tkatchenko, and K.-R. Müller, *J. Chem. Phys.* **148**, 241722 (2018).

²² K. Schütt, P.-J. Kindermans, H. E. S. Felix, S. Chmiela, A. Tkatchenko, and K.-R. Müller, in *NIPS* (2017).

²³ R. Sato, arxiv:2003.04078 (2020).

²⁴ C. Morris, M. Ritzert, M. Fey, W. L. Hamilton, J. E. Lenssen, G. Rattan, and M. Grohe, *ArXiv181002244 Cs Stat* (2021).

²⁵ B. Weisfeiler and A. Leman, *NTI Ser.* **2**, 12 (1968).

²⁶ B. L. Douglas, arxiv:1101.5211 (2011).

²⁷ N. Shervashidze and K. M. Borgwardt, in *Proceedings of the 22nd International Conference on Neural Information Processing Systems, NIPS’09* (Curran Associates Inc., Red Hook, NY, USA, 2009) pp. 1660–1668.

²⁸ T. N. Kipf and M. Welling, arXiv preprint arXiv:1609.02907 (2016).

²⁹ N. Shervashidze, P. Schweitzer, E. J. van Leeuwen, K. Mehlhorn, and K. M. Borgwardt, *J. Mach. Learn. Res.* **12**, 2539 (2011).

³⁰ D. K. Duvenaud, D. Maclaurin, J. Iparraguirre, R. Bombarell, T. Hirzel, A. Aspuru-Guzik, and R. P. Adams, in *Advances in Neural Information Processing Systems* (2015) pp. 2224–2232.

³¹ S. Kearnes, K. McCloskey, M. Berndl, V. Pande, and P. Riley, *J Comput Aided Mol Des* **30**, 595 (2016).

³² C. Chen, W. Ye, Y. Zuo, C. Zheng, and S. P. Ong, *Chem. Mater.* **31**, 3564 (2019).

³³ B. Anderson, T. S. Hy, and R. Kondor, in *NeurIPS* (2019) p. 10.

³⁴ K. Choudhary and B. DeCost, *npj Comput Mater* **7**, 185 (2021).

³⁵ D. J. Wales and T. R. Walsh, *The Journal of Chemical Physics* **106**, 7193 (1997).

³⁶ S. Maheshwary, N. Patel, N. Sathyamurthy, A. D. Kulkarni, and S. R. Gadre, *J. Phys. Chem. A* **105**, 10525 (2001).

³⁷ A. D. Becke, *J. Chem. Phys.* **98**, 5648 (1993).

³⁸ Q. Sun, X. Zhang, S. Banerjee, P. Bao, M. Barbry, N. S.

- Blunt, N. A. Bogdanov, G. H. Booth, J. Chen, Z.-H. Cui, J. J. Eriksen, Y. Gao, S. Guo, J. Hermann, M. R. Hermes, K. Koh, P. Koval, S. Lehtola, Z. Li, J. Liu, N. Mardirossian, J. D. McClain, M. Motta, B. Mussard, H. Q. Pham, A. Pulkin, W. Purwanto, P. J. Robinson, E. Ronca, E. R. Sayfutyarova, M. Scheurer, H. F. Schurkus, J. E. T. Smith, C. Sun, S.-N. Sun, S. Upadhyay, L. K. Wagner, X. Wang, A. White, J. D. Whitfield, M. J. Williamson, S. Wouters, J. Yang, J. M. Yu, T. Zhu, T. C. Berkelbach, S. Sharma, A. Y. Sokolov, and G. K.-L. Chan, *J. Chem. Phys.* **153**, 024109 (2020).
- ³⁹ G. Imbalzano, A. Anelli, D. Giofré, S. Klees, J. Behler, and M. Ceriotti, *J. Chem. Phys.* **148**, 241730 (2018).
- ⁴⁰ G. R. Medders, A. W. Götz, M. A. Morales, P. Bajaj, and F. Paesani, *J. Chem. Phys.* **143**, 104102 (2015).
- ⁴¹ T. T. Nguyen, E. Székely, G. Imbalzano, J. Behler, G. Csányi, M. Ceriotti, A. W. Götz, and F. Paesani, *J. Chem. Phys.* **148**, 241725 (2018).
- ⁴² V. Kapil, M. Rossi, O. Marsalek, R. Petraglia, Y. Litman, T. Spura, B. Cheng, A. Cuzzocrea, R. H. Meißner, D. M. Wilkins, B. A. Helfrecht, P. Juda, S. P. Binenvenue, W. Fang, J. Kessler, I. Poltavsky, S. Vandenbrande, J. Wieme, C. Corminboeuf, T. D. Kühne, D. E. Manolopoulos, T. E. Markland, J. O. Richardson, A. Tkatchenko, G. A. Tribello, V. Van Speybroeck, and M. Ceriotti, *Comput. Phys. Commun.* **236**, 214 (2019).
- ⁴³ S. Habershon, T. E. Markland, and D. E. Manolopoulos, *J. Chem. Phys.* **131**, 24501 (2009).
- ⁴⁴ K. T. Schütt, M. Gastegger, A. Tkatchenko, K.-R. Müller, and R. J. Maurer, *Nat Commun* **10**, 5024 (2019).
- ⁴⁵ K. R. Brorsen, *J. Chem. Phys.* **150**, 204104 (2019).
- ⁴⁶ N. Dandu, L. Ward, R. S. Assary, P. C. Redfern, B. Narayanan, I. T. Foster, and L. A. Curtiss, *J. Phys. Chem. A* **124**, 5804 (2020).
- ⁴⁷ J. Westermayr, M. Gastegger, and P. Marquetand, *J. Phys. Chem. Lett.* **11**, 3828 (2020).
- ⁴⁸ J. Westermayr and R. J. Maurer, *Chem. Sci.* **12**, 10755 (2021).
- ⁴⁹ R. Kakarala, *J Math Imaging Vis* **44**, 341 (2012).